

In-Context Source and Channel Coding

Ziqiong Wang, Tianqi Ren, Rongpeng Li, Zhifeng Zhao, and Honggang Zhang

Abstract—Separate Source–Channel Coding (SSCC) remains attractive for text transmission due to its modularity and compatibility with mature entropy coders and powerful channel codes. However, SSCC often suffers from a pronounced cliff effect in low Signal-to-Noise Ratio (SNR) regimes, where residual bit errors after channel decoding can catastrophically break lossless source decoding, especially for Arithmetic Coding (AC) driven by Large Language Models (LLMs). This paper proposes a receiver-side In-Context Decoding (ICD) framework that enhances SSCC robustness without modifying the transmitter. ICD leverages an Error Correction Code Transformer (ECCT) to obtain bit-wise reliability for the decoded information bits. Based on the context-consistent bitstream, ICD constructs a confidence-ranked candidate pool via reliability-guided bit flipping, samples a compact yet diverse subset of candidates, and applies an LLM-based arithmetic decoder to obtain both reconstructions and sequence-level log-likelihoods. A reliability–likelihood fusion rule then selects the final output. We further provide theoretical guarantees on the stability and convergence of the proposed sampling procedure. Extensive experiments over Additive White Gaussian Noise (AWGN) and Rayleigh fading channels demonstrate consistent gains compared with conventional SSCC baselines and representative Joint Source-Channel Coding (JSCC) schemes.

Index Terms—Separate Source–Channel Coding (SSCC), LLM-based arithmetic coding, Error Correction Code Transformer (ECCT), context-consistent decoding, candidate processing pipeline.

I. INTRODUCTION

In recent years, Semantic Communications (SemCom) have attracted growing attention [1]–[4], driven by the need to deliver task-relevant meaning rather than faithfully transporting raw symbols, and further accelerated by advances in deep learning and generative models [5]. While deep learning-based Joint Source-Channel Coding (JSCC) enables end-to-end semantic-aware transceivers with robustness under finite blocklength and time-varying channels [6]–[12], Separate Source-Channel Coding (SSCC) remains attractive due to its modularity and standard compliance [13]–[15]. By decoupling source coding and channel coding, SSCC can directly reuse mature compressors [16] and capacity-approaching channel codes [17], and in principle achieves near-error-free, bit-exact reconstruction at sufficiently high Signal-to-Noise Ratio (SNR). Meanwhile, motivated by the prediction-compression duality [18], modern neural predictors, ranging from recurrent and hybrid compressors [19]–[21] to LLM-based

Z. Wang, T. Ren and R. Li are with the College of Information Science and Electronic Engineering, Zhejiang University (email: {wangziqiong, rentianqi, lirongpeng}@zju.edu.cn).

Z. Zhao is with Zhejiang Lab as well as the College of Information Science and Electronic Engineering, Zhejiang University (email: zhaozf@zhejianglab.com).

H. Zhang is with the Macau University of Science and Technology, China (email: honggang.zhang@ieee.org).

schemes [22]–[26], can benefit the source encoders such as Huffman coding [27] and arithmetic coding [28], yielding improved transmission efficiency. However, though Large Language Model (LLM)-based SSCC could bring superior performance than JSCC [13], it suffers from the severe “cliff effect”, whereby the performance degrades sharply in low-SNR regimes. This degradation primarily arises because even a small number of residual bit errors after channel decoding may catastrophically break subsequent source decoding.

There is no doubt that to improve robustness in low-SNR regimes, SSCC can resort to enhancing the channel-coding side [29]–[35]. However, under finite blocklength and stringent latency constraints, closing the gap to optimal decoding remains challenging. Learning-aided decoders have been explored, including model-based designs [36]–[43] and model-free approaches [44]–[47]. Notably, the Error Correction Code Transformer (ECCT) [48] has incorporated code-aware inductive biases via parity-check-guided masked self-attention and has achieved error-rate improvements in low-SNR conditions. Nevertheless, such decoders remain constrained by channel observations alone [49], without introducing explicit external information.

On the other hand, leveraging contextual information [50]–[52] at the receiver offers a backward-compatible means to enhance robustness without violating existing SSCC architectures. However, directly applying in-context decoding to corrupted bitstreams is often insufficient, as early decoding errors can dominate the inference process and lead to unstable or suboptimal reconstructions. To address this limitation, a natural approach is to maintain multiple candidates during decoding [53], perform backtracking [54], or introduce diversity through stochastic sampling [55]. However, exhaustively exploring the candidate space is computationally prohibitive when expensive LLM-based decoding [13] is involved, while unconstrained sampling may generate redundant or low-quality candidates. In principle, both in-context information and channel decoding reliability can contribute to maintaining a compact yet diverse set of plausible candidates for improved decoding performance.

In this paper, we propose in-context source and channel coding for SSCC-based transmission, aiming to mitigate the cliff effect. Particularly, we calibrate a receiver-side In-Context Decoding (ICD) framework that augments a standard SSCC pipeline by coupling ECCT-assisted channel decoding with LLM-driven arithmetic source decoding in a lightweight manner. Here, ECCT provides a bit-wise reliability vector that identifies probabilistically corrupted positions, while in-context information, delivered through previous transmissions and/or other reliable channels, offers a strong prior to reduce

ambiguity in the recovered message. Based on the channel-decoded bitstream, its reliability vector, and the contextual bits, we leverage In-Context Candidate Generator (CCG) to construct a confidence-ranked candidate pool through reliability-guided bit flipping. Afterward, to balance the computational budget and decoding accuracy, we adopt In-Context Candidate Sampler (CCS), which selects a sufficiently compact yet highly plausible subset of candidates and their sequence-level log-likelihoods for LLM-based source decoding. Finally, we adopt In-Context Likelihood Ranking (CLR) to select the most plausible reconstruction by jointly accounting for ECCT-derived reliability and linguistic plausibility. Besides the key distinctions with representative prior studies in Table I, we summarize our contributions as follows.

- We introduce a practical in-context source and channel coding mechanism that incorporates contextual information into the SSCC receiver and explicitly maintains context consistency via an overwrite-based step, thereby constraining the feasible message space and improving robustness without modifying the transmitter.
- We develop a three-stage candidate processing pipeline through leveraging the ECCT-provided bit-wise reliability. Specifically, we employ CCG to construct a confidence-ranked set of candidate bitstreams via reliability-guided bit flipping. To achieve a favorable accuracy-complexity trade-off, we further apply CCS to select a compact yet diverse subset. Finally, we use CLR to integrate the ECCT-derived reliability with the LLM decoding log-likelihood to determine the final reconstruction. Moreover, we provide theoretical guarantees on the stability and convergence of the proposed CCS module.
- We conduct extensive evaluations and demonstrate the superiority of ICD over conventional SSCC baselines, represented by Huffman-SSCC and ECCT-aided scheme [13], as well as over representative JSCC schemes, including DeepSC [56], Universal Transformer (UT) [57], and UT with quantization [58].

The remainder of the paper is organized as follows. Sec. II succinctly reviews the key components of our SSCC system. Sec. III briefly introduces the system model and formulates the problem. Sec. IV presents the overview of our proposed ICD framework. In Sec. V, we elaborate on the experimental results and discussions. Finally, Sec. VI concludes the paper. For convenience, we list the major notations of this paper in Table II.

II. PRELIMINARIES

A. LLM-based Source Coding

We consider LLM-based Arithmetic Coding (AC) [28] for source coding [13]. For a tokenizer vocabulary $\mathcal{D} = \{D_1, \dots, D_\tau\}$, a pre-trained LLM can map a source sequence \mathbf{s} to a token sequence $\mathbf{t}_{1:N_t}$ with $t_k \in \mathcal{D}$, while providing token-level conditional probabilities $\tilde{p}(t_k \mid \mathbf{t}_{1:k-1})$ for generation. Using these conditionals, AC maps $\mathbf{t}_{1:N_t}$ to a binary message $\mathbf{m} \in \{0, 1\}^K$. By progressively updating a probability

interval by the autoregressive structure of the LLM, the source can eventually be encoded with a minimal number of bits¹.

At the receiver, given a channel-decoded bitstream estimate $\hat{\mathbf{m}}$ and the same LLM, an arithmetic decoder gradually locates the most appropriate interval corresponding to a token sequence $\tilde{\mathbf{t}}$ and deterministically recovers the reconstructed text $\tilde{\mathbf{s}}$. Beyond producing the reconstruction, the LLM also yields a sequence-level plausibility for the decoded sequence by accumulating token log-probabilities along the decoding path:

$$\ell(\tilde{\mathbf{t}}) \triangleq \sum_{k=1}^{|\tilde{\mathbf{t}}|} \log \tilde{p}(\tilde{t}_k \mid \tilde{\mathbf{t}}_{1:k-1}). \quad (1)$$

For convenience, we denote the transmitter-side LLM-driven arithmetic encoding operation by $\mathcal{F}_{\text{LLM}_s}(\cdot)$ and the receiver-side arithmetic decoding and likelihood evaluation operation by $\mathcal{F}_{\text{LLM}_r}(\cdot)$.

B. Error Correction Code Transformer

We adopt the ECCT² [48] as a receiver-side reliability estimation module to quantify bit-wise confidence under severe noise. Without loss of generality, assume that for a Binary Phase-Shift Keying (BPSK)-coded sequence $\mathbf{x}_s \in \{\pm 1\}^N$, the corresponding channel output can be written as:

$$\mathbf{y} = h\mathbf{x}_s + \mathbf{z}, \quad \mathbf{z} \sim \mathcal{N}(\mathbf{0}, \sigma_n^2 \mathbf{I}), \quad (2)$$

where h is the Additive White Gaussian Noise (AWGN) or Rayleigh fading coefficient, and $\mathbf{z} \sim \mathcal{N}(\mathbf{0}, \sigma_n^2 \mathbf{I})$ represents additive Gaussian noise. Following [48], the channel observation can also be expressed in a multiplicative form $\mathbf{y} = \mathbf{x}_s \odot \tilde{\mathbf{z}}$, where $\tilde{\mathbf{z}} \in \mathbb{R}^N$ denotes an equivalent multiplicative disturbance.

We consider a binary linear block code of length N and dimension K characterized by a parity-check matrix $\mathbf{H} \in \{0, 1\}^{(N-K) \times N}$ (e.g., an Low-Density Parity-Check (LDPC) code). Then, given the real-valued channel output $\mathbf{y} \in \mathbb{R}^N$, ECCT exploits the code constraints \mathbf{H} via the binary syndrome computed from a hard-decision mapping. Specifically, define the syndrome vector as:

$$\text{syn}(\mathbf{y}) \triangleq \mathbf{H} \text{sign_to_bin}(\mathbf{y}) \pmod{2} \in \{0, 1\}^{N-K}, \quad (3)$$

where $\text{sign_to_bin}(\mathbf{y}) \triangleq \frac{1}{2}(\mathbf{1} - \text{sign}(\mathbf{y})) \in \{0, 1\}^N$ while $\text{syn}(\mathbf{y}) = \mathbf{0}$ indicates that the hard-decision codeword satisfies all parity checks. To jointly incorporate soft channel observations and code-structure information, ECCT forms an augmented input feature vector:

$$\hat{\mathbf{y}} \triangleq [|\mathbf{y}|, \text{syn}(\mathbf{y})] \in \mathbb{R}^{2N-K}. \quad (4)$$

ECCT processes $\hat{\mathbf{y}}$ and outputs an estimate of the disturbance:

$$\hat{\mathbf{z}} = \mathcal{F}_{\text{ECCT}}(\hat{\mathbf{y}}), \quad (5)$$

¹The standard AC interval updates and the corresponding LLM-AC decoding steps can be found in [13].

²Complete architectural and training details of ECCT can be found in [48].

TABLE I
SUMMARY AND COMPARISON OF RELATED PAPERS.

References	LLM Source Decoding	In-Context Information	Reliability-Enhanced Channel Decoding	Brief Description
Zhou F, <i>et al.</i> [59]	○	●	○	Using a shared knowledge base for semantic abstraction and recovery.
Choukroun Y, <i>et al.</i> [48]	○	○	●	Improving channel decoding with a transformer-based ECCT decoder.
Kurmukova A, <i>et al.</i> [60]	○	○	●	Boosting decoder reliability via transmitter-side friendly perturbations.
Ren T, <i>et al.</i> [13]	●	○	●	Combining ECCT-aided channel decoding with LLM-based lossless source decoding.
This paper	●	●	●	Performing in-context, reliability-guided candidate decoding with LLM-based source decoding.

Notations: ● indicates fully included; ○ means partially included; ○ denotes not included.

TABLE II
MAJOR NOTATIONS USED IN THIS PAPER.

Notation	Definition
$\mathbf{s}_{1:N_s}, N_s$	Input text sequence and its length.
$\mathbf{t}_{1:N_t}, N_t$	Token sequence produced by the LLM tokenizer and its length.
$\mathbf{m}, \hat{\mathbf{m}}$	Source-coded message and its channel-decoded version.
$\mathbf{x}_b, \mathbf{x}_s$	Channel-coded binary codeword and its BPSK-modulated symbol sequence.
N, K	Codeword length and message length of channel code.
$\mathcal{D} = \{D_1, \dots, D_\tau\}$	Token vocabulary defined by the tokenizer and τ is the vocabulary size.
$\tilde{p}(\cdot)$	LLM-induced conditional probability used as the distribution for AC.
\mathbf{G}, \mathbf{H}	Generator matrix and parity check matrix.
h	Channel fading coefficient.
$\mathbf{z}, \hat{\mathbf{z}}$	Additive Gaussian noise and ECCT output estimating the multiplicative disturbance.
σ_n^2, \mathbf{I}	Noise variance and identity matrix in the Gaussian noise model.
\mathbf{y}	Received real-valued channel output vector.
$\tilde{\mathbf{y}}$	ECCT input feature vector (i.e., concatenation of magnitude and syndrome features of \mathbf{y}).
f_k	Bit-flip indicator when constructing the candidate $\tilde{\mathbf{m}}$.
$\boldsymbol{\rho}$	Normalized bit-wise reliability vector obtained by applying sigmoid to $\hat{\mathbf{z}}$.
ρ_m	Bit-wise reliability vector for the information bits.
$\tilde{\rho}_m$	Candidate-specific reliability associated with $\tilde{\mathbf{m}}$.
ℓ	Sequence-level log-likelihood of the LLM-decoded candidate.
$\hat{\mathbf{x}}_s, \hat{\mathbf{x}}_b$	ECCT-processed soft symbol estimate and hard-decision demodulated estimate.
\mathbf{m}_{pre}	Contextual information bit sequence.
$\tilde{\mathbf{m}}$	Candidate bitstream generated by applying a specific bit-flip pattern to \mathbf{m} .
$\tilde{\mathbf{s}}$	Reconstructed text sequence by the LLM-based source decoder from candidate bitstream $\tilde{\mathbf{m}}$.
$\tilde{\mathbf{s}}^*$	Final reconstructed text sequence.
\mathcal{M}_{L_c}, L_c	Candidate set retained by CCG and its size.
\mathcal{M}_{L_s}, L_s	Subset sampled by CCS and its size.
Ω	State space consisting of all subsets of \mathcal{M}_{L_c} with fixed cardinality L_s .
$\mathcal{S}^{(t)}$	State of the Markov chain at iteration t , represented as a subset of \mathcal{M}_{L_c} .
$E(\cdot)$	Energy function evaluating the quality of subset in terms of reliability and diversity.
$\pi(\cdot)$	Target probability distribution over the state space Ω .

which implicitly captures position-dependent decoding uncertainty while respecting parity-check consistency. On this basis, ECCT computes a recovered BPSK-coded sequence by

$$\hat{\mathbf{x}}_s = \text{sign_to_bin}(\mathbf{y} \odot \hat{\mathbf{z}}) \in \{0, 1\}^N. \quad (6)$$

In this work, we further convert $\hat{\mathbf{z}}$ into a bit-wise reliability vector:

$$\boldsymbol{\rho} = \sigma(\hat{\mathbf{z}}) \in [0, 1]^N, \quad (7)$$

where a larger ρ_d indicates higher confidence on the accuracy of the d -th decoded bit. The reliability $\boldsymbol{\rho}$ is used as the common input to the subsequent ICD modules to guide candidate construction and selection.

III. SYSTEM MODEL AND PROBLEM FORMULATION

A. System Model

We consider an SSCC-based text transmission framework in which the receiver is augmented with ECCT-assisted channel decoding and an LLM-based source decoder equipped with ICD, which comprises CCG, CCS, and CLR, in addition to conventional source and channel coding, modulation, and demodulation. Fig. 1 shows the corresponding system block diagram.

For the input text sequence $\mathbf{s}_{1:N_s}$, a lossless source encoder compresses it into a binary message:

$$\mathbf{m} = \mathcal{F}_{\text{LLM}_s}(\mathbf{s}_{1:N_s}) \in \{0, 1\}^K, \quad (8)$$

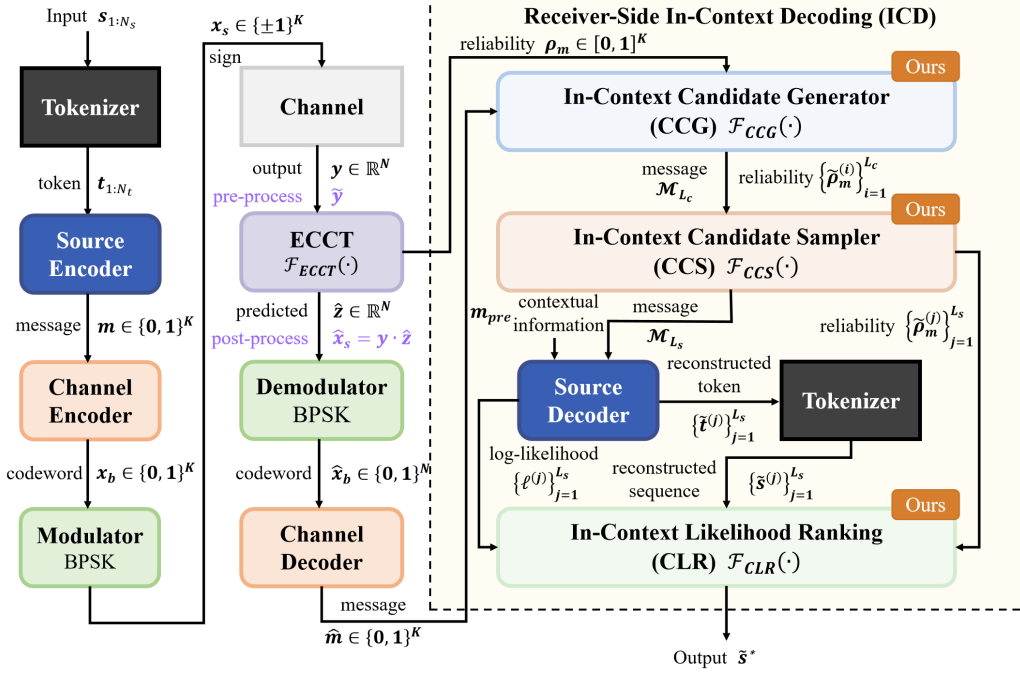


Fig. 1. Framework of the Proposed ICD-Aided SSCC System.

where as mentioned in Sec. II-A, $\mathcal{F}_{LLM_s}(\cdot)$ denotes a LLM-compatible source encoder that maps text into a length- K bitstream through tokenization and probability-driven AC. The same pipeline can also be applied to other discrete sources (e.g., images) after appropriate lossless formatting or compression.

The message \mathbf{m} is then protected by an (N, K) LDPC channel code as:

$$\mathbf{x}_b = \mathbf{m}\mathbf{G} \pmod{2} \in \{0, 1\}^N, \quad (9)$$

where $\mathbf{G} \in \{0, 1\}^{K \times N}$ is the generator matrix. The corresponding parity-check matrix $\mathbf{H} \in \{0, 1\}^{(N-K) \times N}$ satisfies:

$$\mathbf{G}\mathbf{H}^\top = \mathbf{0}. \quad (10)$$

Notably, other error correction codes such as Polar codes [32] can be applied as well [48]. The binary codeword \mathbf{x}_b is modulated via BPSK into $\mathbf{x}_s = 1 - 2\mathbf{x}_b \in \{\pm 1\}^N$ and transmitted over the channel, as defined in Eq. (2).

At the receiver, ECCT takes the real-valued channel output \mathbf{y} and the code constraints as input, and produces a recovered BPSK-coded sequence $\hat{\mathbf{x}}_s$, an estimate of disturbance $\hat{\mathbf{z}}$, and a bit-wise reliability vector $\rho \in [0, 1]^N$ as described in Sec. II-B. Hence, hard-decision BPSK demodulation yields the binary codeword estimate:

$$\hat{\mathbf{x}}_b = \text{sign_to_bin}(\hat{\mathbf{x}}_s) \in \{0, 1\}^N. \quad (11)$$

In this work, we adopt a systematic channel encoder, such that the information bits occupy the first K positions of the codeword. Since ECCT operates as a channel decoder

producing an estimated codeword, recovering the information bitstream reduces to extracting the first K bits:

$$\hat{\mathbf{m}} = \hat{\mathbf{x}}_{b,1:K} \in \{0, 1\}^K, \quad (12)$$

Similarly, since the ECCT-derived reliability $\rho \in [0, 1]^N$ is defined at the codeword-bit level, we take its subvector aligned with the information positions:

$$\rho_{\mathbf{m}} = \rho_{1:K} \in [0, 1]^K. \quad (13)$$

Given the channel decoding result $\hat{\mathbf{m}}$, as mentioned in Sec. II-A, an LLM-based source decoder $\mathcal{F}_{LLM_r}(\cdot)$ can eventually produce a reconstructed sequence $\tilde{\mathbf{s}}$, along with its linguistic log-likelihood ℓ :

$$(\tilde{\mathbf{s}}, \ell) = \mathcal{F}_{LLM_r}(\hat{\mathbf{m}}). \quad (14)$$

B. Problem Formulation

Conventional SSCC systems often suffer from a *cliff effect* in low-SNR scenarios, where crossing below a specific SNR threshold triggers an abrupt rise in the bit error rate and a severe drop in reconstruction fidelity, as illustrated by the second black line in Fig. 4 and Fig. 5. The primary reason lies in the fact that an incorrect early bit can shift the LLM-based decoder to a wrong sub-interval for arithmetic decoding, which then perturbs subsequent token boundary decisions and triggers error propagation across many tokens. Consequently, even a small number of residual bit errors after channel decoding may catastrophically break lossless source decoding.

To improve reliability under such unfavorable conditions, we consider receiver-side enhancements that utilize additional contextual information \mathbf{m}_{pre} , which has been obtained through

previous transmissions and/or other reliable channels [61]–[63]. More clearly, we argue that the in-context information \mathbf{m}_{pre} can provide a strong probabilistic prior that helps combat the arising severe noise. In other words, if we can construct multiple candidate bitstreams $\tilde{\mathbf{m}}$ from the channel decoding result $\hat{\mathbf{m}}$, it will benefit the receiver by evaluating the contextual plausibility (i.e., log-likelihood) ℓ of one bit stream and determining the superior one. To support such an intuition, a confidence-ranked candidate set shall be computed from the available contextual information:

$$\left(\mathcal{M}_{L_c}, \{\tilde{\rho}_{\text{m}}^{(i)}\}_{i=1}^{L_c}\right) = \mathcal{F}_{\text{CCG}}(\hat{\mathbf{m}}, \rho_{\text{m}}; L_c), \quad (15)$$

where $\mathcal{F}_{\text{CCG}}(\cdot)$ denotes a CCG function, while $\mathcal{M}_{L_c} = \{\tilde{\mathbf{m}}^{(i)}\}_{i=1}^{L_c}$ denotes the top- L_c candidate bitstreams retained according to the ECCT-derived bit-wise reliability.

However, if all candidates go through the LLM, it will incur substantial computational cost. To better balance cost and diversity, it becomes appealing to design a sampling module $\mathcal{F}_{\text{CCS}}(\cdot)$ that selects L_s candidates from \mathcal{M}_{L_c} :

$$\left(\mathcal{M}_{L_s}, \{\tilde{\rho}_{\text{m}}^{(j)}\}_{j=1}^{L_s}\right) = \mathcal{F}_{\text{CCS}}\left(\mathcal{M}_{L_c}, \{\tilde{\rho}_{\text{m}}^{(i)}\}_{i=1}^{L_c}; L_s\right), \quad (16)$$

with $\mathcal{M}_{L_s} = \{\tilde{\mathbf{m}}^{(j)}\}_{j=1}^{L_s}$ and $L_s \leq L_c - 2$. Each selected candidate is then fed into the LLM-based source decoder $\mathcal{F}_{\text{LLM}_r}(\cdot)$, producing a reconstructed sequence and its log-likelihood:

$$\left(\tilde{\mathbf{s}}^{(j)}, \ell^{(j)}\right) = \mathcal{F}_{\text{LLM}_r}\left(\tilde{\mathbf{m}}^{(j)}; \mathbf{m}_{\text{pre}}\right), \quad j = 1, \dots, L_s. \quad (17)$$

Finally, the ECCT-derived bit-wise reliability and linguistic log-likelihood can undergo a CLR \mathcal{F}_{CLR} for output the final reconstruction:

$$\tilde{\mathbf{s}}^* = \mathcal{F}_{\text{CLR}}\left(\{\tilde{\mathbf{s}}^{(j)}\}_{j=1}^{L_s}, \{\ell^{(j)}\}_{j=1}^{L_s}, \{\tilde{\rho}_{\text{m}}^{(j)}\}_{j=1}^{L_s}\right), \quad (18)$$

where $\mathcal{F}_{\text{CLR}}(\cdot)$ implements a generic confidence–likelihood fusion rule and returns the optimal candidate $\tilde{\mathbf{s}}^*$ as the decoding result.

For notational convenience, we denote the decoder by $\Phi(\cdot) = \mathcal{F}_{\text{CLR}} \circ \mathcal{F}_{\text{LLM}_r} \circ \mathcal{F}_{\text{CCS}} \circ \mathcal{F}_{\text{CCG}}(\cdot)$. Our goal is to design a computationally efficient source and channel decoder $\Phi(\cdot)$ that maps the ECCT-assisted decoding output ρ_m , the channel decoding result $\hat{\mathbf{m}}$, and the contextual side information \mathbf{m}_{pre} to the final reconstruction $\hat{\mathbf{s}}^*$.

$$\begin{aligned} & \min \mathbb{E}[d(\mathbf{s}_{1:N_s}, \tilde{\mathbf{s}}^*)] \\ \text{s.t. } & \text{Cost}(\mathcal{F}_{\text{CCS}} \circ \mathcal{F}_{\text{LLM}_r}) \leq \mathcal{B}, \quad \tilde{\mathbf{s}}^* = \Phi(\hat{\mathbf{m}}, \rho_{\text{m}}, \mathbf{m}_{\text{pre}}), \end{aligned} \quad (19)$$

where $d(\cdot, \cdot)$ measures the reconstruction mismatch, and $\text{Cost}(\mathcal{F}_{\text{CCS}} \circ \mathcal{F}_{\text{LLM}_r})$ denotes the expected computational cost of LLM decoding, which is proportional to the number of candidates eventually sampled by \mathcal{F}_{CCS} . We leave the design of the modules in ICD in Sec. IV.

IV. THE FRAMEWORK OF ICD

Fig. 2 illustrates the overall framework of the proposed ICD.

A. In-Context Candidate Generator

The role of CCG is to produce a confidence-ranked candidate set for the information-bit sequence. Given the channel decoding output $\hat{\mathbf{m}} \in \{0, 1\}^K$, we construct a candidate set $\mathcal{M} \triangleq \{\tilde{\mathbf{m}}^{(d)}\}_{d=1}^{2^K}$ by enumerating all possible bit-flip patterns. Specifically, let $\mathbf{f}^{(d)} = [f_1^{(d)}, \dots, f_K^{(d)}] \in \{0, 1\}^K$ denote the d -th flip pattern, where $f_p^{(d)} = 1$ indicates flipping the p -th bit and $f_p^{(d)} = 0$ otherwise, with $d = 1, \dots, 2^K$. Given $\mathbf{f}^{(d)}$, the corresponding candidate bitstream $\tilde{\mathbf{m}}^{(d)} \in \mathcal{M}$ is constructed entry-wise as:

$$\tilde{m}_p^{(d)} = \hat{m}_p \oplus f_p^{(d)}, \quad p = 1, \dots, K, \quad (20)$$

where \oplus denotes the XOR operation.

Given the ECCT-derived bit-wise reliability vector $\rho_{\text{m}} = [\rho_{\text{m},1}, \dots, \rho_{\text{m},K}] \in [0, 1]^K$, we define the candidate-specific reliability as $\tilde{\rho}_{\text{m}}^{(d)} = [\tilde{\rho}_{\text{m},1}^{(d)}, \dots, \tilde{\rho}_{\text{m},K}^{(d)}]$, whose p -th entry under candidate $\tilde{\mathbf{m}}^{(d)}$ can be computed as:

$$\tilde{\rho}_{\text{m},p}^{(d)} = (1 - f_p^{(d)}) \rho_{\text{m},p} + f_p^{(d)} (1 - \rho_{\text{m},p}), \quad p = 1, \dots, K. \quad (21)$$

Accordingly, the aggregate confidence score of candidate $\tilde{\mathbf{m}}^{(d)}$ is defined as:

$$\mathcal{F}_{\text{Conf}}\left(\tilde{\mathbf{m}}^{(d)}\right) = \sum_{p=1}^K \tilde{\rho}_{\text{m},p}^{(d)}, \quad d = 1, \dots, 2^K. \quad (22)$$

Finally, CCG retains the top- L_c candidates with the largest confidence scores, yielding a confidence-ranked candidate set:

$$\mathcal{M}_{L_c} = \left\{ \tilde{\mathbf{m}}^{(i)} \mid i \in \arg \max_{L_c, 1 \leq d \leq 2^K} \mathcal{F}_{\text{Conf}}(\tilde{\mathbf{m}}^{(d)}) \right\} \quad i = 1, \dots, L_c. \quad (23)$$

B. In-Context Candidate Sampler

CCG leverages the ECCT-derived bit reliability to score candidate bitstreams and efficiently prune an exponentially large flip space, resulting in a confidence-ranked set of top- L_c candidates. While this confidence-guided pruning is essential for computational tractability, the resulting ranking is inevitably affected by reliability miscalibration, as evidenced by Fig. 3, which shows that a non-negligible number of erroneous bits persist even in high-confidence regimes. Moreover, candidates with high confidence scores are often generated by flipping similar subsets of low-reliability bits, leading to strong correlations among top-ranked candidates and consequently small pairwise Hamming distances.

As a consequence, directly truncating the ranked list to the top- L_s candidates would produce a highly concentrated and redundant subset, severely limiting the effective exploration space available to the downstream LLM-based decoder. To address this issue, CCS performs diversity-preserving subset selection by explicitly balancing aggregate confidence and inter-candidate Hamming diversity, so that with a limited number of LLM decoding attempts L_s , the selected candidates span multiple plausible error patterns and substantially increase the probability of including a decodable or correct bitstream.

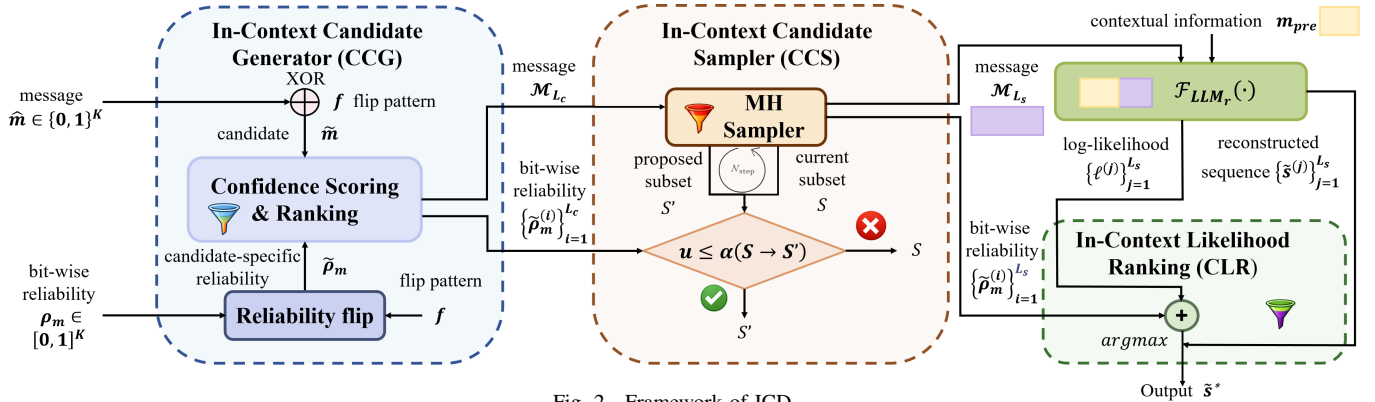


Fig. 2. Framework of ICD.

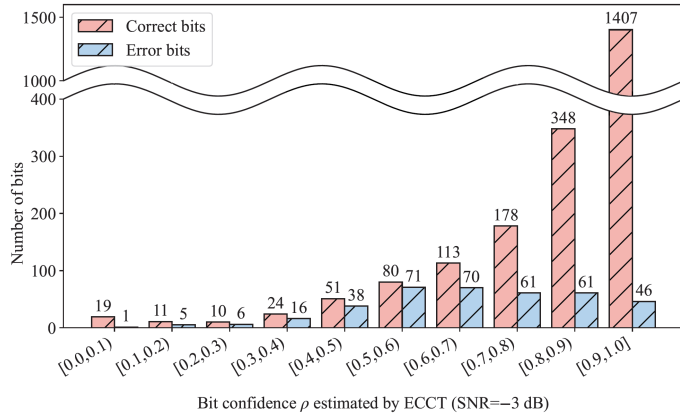


Fig. 3. Distribution of correct and erroneous bits across confidence levels.

This subset-level trade-off naturally leads to a large search space. For typical values of L_c and L_s , the number of feasible subsets scales as $\binom{L_c}{L_s}$, making exhaustive evaluation costly in practice. This motivates the use of approximate methods that can efficiently explore the subset space without incurring prohibitive computational overhead. To this end, CCS adopts a sampling-based approach inspired by Metropolis-Hastings (MH) [64], [65], which enables efficient exploration of the subset space with a controllable computational budget while naturally introducing randomness to promote diversity.

Specifically, CCS formulates the subset selection problem as sampling from a structured probability distribution defined over subsets of \mathcal{M}_{L_c} . To this end, we construct a Markov chain $\{\mathcal{S}^{(t)}\}_{t \geq 0}$ on the state space $\Omega \triangleq \{\mathcal{S} \subseteq \mathcal{M}_{L_c} \mid |\mathcal{S}| = L_s\}$, where each state $\mathcal{S}^{(t)} \in \Omega$ is a candidate subset of fixed cardinality L_s to be forwarded to the subsequent LLM-based decoding stage. Subsequently, we define the target distribution over Ω as:

$$\pi(\mathcal{S}) = \exp(-\beta E(\mathcal{S})), \quad \mathcal{S} \in \Omega, \quad (24)$$

where $\beta > 0$ controls the sharpness and the energy $E(\mathcal{S})$ jointly captures ECCT-derived reliability and inter-candidate

diversity, given by

$$E(\mathcal{S}) = - \sum_{\tilde{\mathbf{m}} \in \mathcal{S}} \mathcal{F}_{\text{Conf}}(\tilde{\mathbf{m}}) - \lambda \sum_{\substack{\tilde{\mathbf{m}}, \tilde{\mathbf{m}}' \in \mathcal{S} \\ \tilde{\mathbf{m}} \neq \tilde{\mathbf{m}}'}} \mathcal{F}_{\text{Hamming}}(\tilde{\mathbf{m}}, \tilde{\mathbf{m}}'), \quad (25)$$

where $\mathcal{F}_{\text{Conf}}(\cdot)$ denotes the ECCT-derived aggregate confidence while $\mathcal{F}_{\text{Hamming}}(\cdot)$ measures pairwise Hamming distance, and $\lambda \geq 0$ balances reliability preservation and diversity encouragement.

Given the current state $\mathcal{S} \in \Omega$, we generate a proposal state $\mathcal{S}' \in \Omega$ via a single replacement move $\mathcal{S}' = (\mathcal{S} \setminus \{\tilde{\mathbf{m}}\}) \cup \{\tilde{\mathbf{m}}''\}$, by changing a uniformly sampled $\tilde{\mathbf{m}} \in \mathcal{S}$ to $\tilde{\mathbf{m}}'' \in (\mathcal{M}_{L_c} \setminus \mathcal{S})$, where \setminus denotes the set difference operator. This defines the proposal distribution:

$$q(\mathcal{S}' | \mathcal{S}) = \frac{1}{L_s (L_c - L_s)}, \quad (26)$$

and $q(\mathcal{S}' | \mathcal{S}) = q(\mathcal{S} | \mathcal{S}')$ holds due to the symmetry of the replacement move.

The Markov chain transition kernel P is then induced by the MH accept-reject rule:

$$P(\mathcal{S}' | \mathcal{S}) = q(\mathcal{S}' | \mathcal{S}) \alpha(\mathcal{S} \rightarrow \mathcal{S}'), \quad \mathcal{S}' \neq \mathcal{S}, \quad (27)$$

with acceptance probability:

$$\alpha(\mathcal{S} \rightarrow \mathcal{S}') = \min \left\{ 1, \frac{\pi(\mathcal{S}') q(\mathcal{S} | \mathcal{S}')}{\pi(\mathcal{S}) q(\mathcal{S}' | \mathcal{S})} \right\}$$

$$\begin{aligned}
&= \min \left\{ 1, \frac{\pi(\mathcal{S}')}{\pi(\mathcal{S})} \right\} \\
&= \min \{ 1, \exp(-\beta[E(\mathcal{S}') - E(\mathcal{S})]) \}. \quad (28)
\end{aligned}$$

A uniform random number $u \sim \mathcal{U}(0, 1)$ is then drawn, and the proposal is accepted if $u \leq \alpha(\mathcal{S} \rightarrow \mathcal{S}')$. Otherwise, the chain remains at \mathcal{S} . For completeness, the self-transition probability is:

$$P(\mathcal{S}|\mathcal{S}) = 1 - \sum_{\mathcal{S}' \in \Omega, \mathcal{S}' \neq \mathcal{S}} P(\mathcal{S}'|\mathcal{S}). \quad (29)$$

After a fixed number of MH iterations N_{step} , CCS outputs a sampled subset \mathcal{M}_{L_s} of size L_s , which exhibits both high aggregate confidence and sufficient diversity across candidate bitstreams. This sampling-enhanced selection avoids excessive concentration on highly similar candidates that arise from correlated low-confidence bit flips, while maintaining tractable computational complexity.

Definition 1 (Stationarity under Detailed Balance [66]). Let $\{\mathcal{S}^{(t)}\}_{t \geq 0}$ be a Markov chain on a finite state space Ω with transition kernel P . If there exists a distribution π such that the detailed balance condition holds

$$\pi(\mathcal{S}) P(\mathcal{S}'|\mathcal{S}) = \pi(\mathcal{S}') P(\mathcal{S}|\mathcal{S}'), \quad \forall \mathcal{S}, \mathcal{S}' \in \Omega, \quad (30)$$

then π is a stationary distribution of the Markov chain.

Theorem 1 (Properties of CCS). Consider the Markov chain $\{\mathcal{S}^{(t)}\}_{t \geq 0}$ induced by the CCS sampler on the state space Ω , it satisfies the following properties: (1) The state space Ω is finite. (2) The transition kernel P meets the detailed balance condition with respect to the target distribution π . (3) The Markov chain is irreducible and aperiodic on Ω .

Proof.

- *Finite state space:* Since \mathcal{M}_{L_c} contains exactly L_c candidates, the number of distinct subsets of size L_s is $|\Omega| = \binom{L_c}{L_s}$, which is a finite integer for $0 < L_s < L_c$.
- *Detailed balance:* Without loss of generality, we consider two states \mathcal{S} and \mathcal{S}' , which satisfy $E(\mathcal{S}') \leq E(\mathcal{S})$, thus $\alpha(\mathcal{S} \rightarrow \mathcal{S}') = 1$ and $\alpha(\mathcal{S}' \rightarrow \mathcal{S}) = \exp(-\beta[E(\mathcal{S}') - E(\mathcal{S})])$. Therefore,

$$\begin{aligned}
\pi(\mathcal{S}) P(\mathcal{S}'|\mathcal{S}) &= \pi(\mathcal{S}) q(\mathcal{S}'|\mathcal{S}) \alpha(\mathcal{S} \rightarrow \mathcal{S}') \\
&= \pi(\mathcal{S}) q(\mathcal{S}'|\mathcal{S}) \\
&= \exp(-\beta E(\mathcal{S})) q(\mathcal{S}'|\mathcal{S}). \quad (31)
\end{aligned}$$

On the other hand,

$$\begin{aligned}
\pi(\mathcal{S}') P(\mathcal{S}|\mathcal{S}') &= \pi(\mathcal{S}') q(\mathcal{S}|\mathcal{S}') \alpha(\mathcal{S}' \rightarrow \mathcal{S}) \\
&= \pi(\mathcal{S}') q(\mathcal{S}|\mathcal{S}') \exp(-\beta[E(\mathcal{S}) - E(\mathcal{S}')]) \\
&= \exp(-\beta E(\mathcal{S})) q(\mathcal{S}|\mathcal{S}). \quad (32)
\end{aligned}$$

Taking account of $q(\mathcal{S}'|\mathcal{S}) = q(\mathcal{S}|\mathcal{S}')$ and comparing (31) and (32), we obtain $\pi(\mathcal{S}) P(\mathcal{S}'|\mathcal{S}) = \pi(\mathcal{S}') P(\mathcal{S}|\mathcal{S}')$.

- *Irreducibility:* By construction, each such move has a positive proposal probability $q(\mathcal{S}'|\mathcal{S})$ and a nonzero acceptance probability $\alpha(\mathcal{S} \rightarrow \mathcal{S}')$. Therefore, \mathcal{S}' is

reachable from \mathcal{S} with a positive probability and the chain is irreducible.

- *Aperiodicity:* For an arbitrary state $\mathcal{S} \in \Omega$, by construction, $P(\mathcal{S}'|\mathcal{S}) > 0$. Then we have the following two cases. In the first case, suppose there exists a state $\mathcal{S}' \in \Omega \setminus \{\mathcal{S}\}$ satisfying $E(\mathcal{S}') > E(\mathcal{S})$ (i.e., an energy-increasing proposal). Then the MH acceptance probability satisfies $\alpha(\mathcal{S} \rightarrow \mathcal{S}') < 1$. Consequently, Eq. (29) can be further written as

$$\begin{aligned}
P(\mathcal{S}|\mathcal{S}) &= \sum_{\mathcal{N} \in \Omega \setminus \{\mathcal{S}\}} q(\mathcal{N}|\mathcal{S}) (1 - \alpha(\mathcal{S} \rightarrow \mathcal{N})) \\
&\stackrel{(a)}{\geq} q(\mathcal{S}'|\mathcal{S}) (1 - \alpha(\mathcal{S} \rightarrow \mathcal{S}')) > 0, \quad (33)
\end{aligned}$$

where \mathcal{N} ranges over all states other than \mathcal{S} in Ω and the inequality (a) is obtained by selecting the term corresponding to \mathcal{S}' in the summation. Therefore, \mathcal{S} has a self-loop, implying that its period is one.

In the second case, for all states $\mathcal{S}' \in \Omega \setminus \{\mathcal{S}\}$, $E(\mathcal{S}') \leq E(\mathcal{S})$. Then, $\alpha(\mathcal{S} \rightarrow \mathcal{S}') = 1$. In this case, $P(\mathcal{S}|\mathcal{S}) = 0$. So if we can find two return paths of co-prime lengths, we will establish aperiodicity by definition.

- *(i) A 2-step return.* Pick any state $\mathcal{S}_1 \in \Omega \setminus \{\mathcal{S}\}$, Note that $E(\mathcal{S}) \geq E(\mathcal{S}_1)$ implies

$$\begin{aligned}
\alpha(\mathcal{S}_1 \rightarrow \mathcal{S}) &= \min \{ 1, \exp(-\beta(E(\mathcal{S}) - E(\mathcal{S}_1))) \} \\
&= \exp(-\beta(E(\mathcal{S}) - E(\mathcal{S}_1))) > 0. \quad (34)
\end{aligned}$$

Thus,

$$\begin{aligned}
P^2(\mathcal{S}|\mathcal{S}) &= \sum_{\mathcal{N} \in \Omega \setminus \{\mathcal{S}\}} P(\mathcal{N}|\mathcal{S}) P(\mathcal{S}|\mathcal{N}) \\
&\stackrel{(b)}{\geq} P(\mathcal{S}_1|\mathcal{S}) P(\mathcal{S}|\mathcal{S}_1) \\
&= q(\mathcal{S}_1|\mathcal{S}) \cdot q(\mathcal{S}|\mathcal{S}_1) \cdot \alpha(\mathcal{S}_1 \rightarrow \mathcal{S}) > 0, \quad (35)
\end{aligned}$$

where the inequality (b) is obtained by selecting the term corresponding to \mathcal{S}_1 in the summation.

- *(ii) A 3-step return.* Given that $L_c \geq L_s + 2$ in our algorithm configuration, we randomly select one distinct elements $a \in \mathcal{S}$ and two distinct candidates $b, c \in \Omega \setminus \mathcal{S}$. Define

$$\begin{aligned}
\mathcal{S}_1 &= (\mathcal{S} \setminus \{a\}) \cup \{b\}, \\
\mathcal{S}_2 &= (\mathcal{S}_1 \setminus \{b\}) \cup \{c\} = (\mathcal{S} \setminus \{a\}) \cup \{c\}. \quad (36)
\end{aligned}$$

Then $\mathcal{S} \rightarrow \mathcal{S}_1 \rightarrow \mathcal{S}_2 \rightarrow \mathcal{S}$ forms a valid three-step transition path of the Markov chain and $\mathcal{S} = (\mathcal{S}_2 \setminus \{c\}) \cup \{a\}$. By construction, $E(\mathcal{S}_1) \leq E(\mathcal{S})$ and hence $\alpha(\mathcal{S} \rightarrow \mathcal{S}_1) = 1$. For the transition $\mathcal{S}_1 \rightarrow \mathcal{S}_2$, the MH acceptance probability satisfies $\alpha(\mathcal{S}_1 \rightarrow \mathcal{S}_2) > 0$, which holds regardless of the ordering between $E(\mathcal{S}_1)$ and $E(\mathcal{S}_2)$.

For the last move, $\alpha(\mathcal{S}_2 \rightarrow \mathcal{S}) > 0$ holds as shown in Eq. (34). Since each corresponding proposal probability is strictly positive, considering the specific three-step return path $\mathcal{S} \rightarrow \mathcal{S}_1 \rightarrow \mathcal{S}_2 \rightarrow \mathcal{S}$ yields

$$P^3(\mathcal{S}|\mathcal{S}) \geq P(\mathcal{S}_1|\mathcal{S}) P(\mathcal{S}_2|\mathcal{S}_1) P(\mathcal{S}|\mathcal{S}_2) > 0. \quad (37)$$

Therefore, $P^2(\mathcal{S}|\mathcal{S}) > 0$ and $P^3(\mathcal{S}|\mathcal{S}) > 0$. Hence, the Markov chain is aperiodic. \blacksquare

This completes the proof. \blacksquare

Lemma 1 (Ergodicity and Convergence [67]). Let $\{\mathcal{S}^{(t)}\}_{t \geq 0}$ be a Markov chain on a finite state space with stationary distribution π . If the chain is irreducible and aperiodic, then π is unique and the distribution of $\mathcal{S}^{(t)}$ converges to π in total variation distance, regardless of the initial state.

Theorem 2 (Stationarity and Convergence of CCS). Consider the Markov chain $\{\mathcal{S}^{(t)}\}_{t \geq 0}$ induced by the CCS sampler. π is the unique stationary distribution, and for any initial state $\mathcal{S}^{(0)}$, the distribution of $\mathcal{S}^{(t)}$ converges to π in total variation distance, that is

$$\lim_{t \rightarrow \infty} \|P^t(\mathcal{S}^{(0)}, \cdot) - \pi(\cdot)\|_{\text{TV}} = 0. \quad (38)$$

Proof. By Theorem 1, the CCS chain operates on a finite state space and satisfies detailed balance with respect to π . Hence, by Definition 1, π is a stationary distribution of the chain. Moreover, Theorem 1 also establishes that the chain is irreducible and aperiodic. Therefore, by Lemma 1, the stationary distribution π is unique and the distribution of $\mathcal{S}^{(t)}$ converges to π in total variation distance for any initial state $\mathcal{S}^{(0)}$. \blacksquare

C. In-Context Likelihood Ranking

For each retained bitstream candidate $\tilde{\mathbf{m}}^{(j)} \in \mathcal{M}_{L_s}$, CLR integrates ECCT-derived reliability with source-level linguistic plausibility to select the final reconstruction. Formally, CLR computes a fused score for each candidate by combining the ECCT-derived reliability profile $\tilde{\rho}_{\mathbf{m}}^{(j)}$ and the LLM log-likelihood $\ell^{(j)}$, and outputs:

$$\tilde{\mathbf{s}}^* = \tilde{\mathbf{s}}^{(j*)}, \quad j^* = \arg \max_{1 \leq j \leq L_s} \left\{ \mathcal{F}_{\text{Conf}}\left(\tilde{\mathbf{m}}^{(j)}\right) + \alpha \ell^{(j)} \right\}, \quad (39)$$

In summary, the pseudocode of the proposed receiver-side ICD procedure is provided in Algorithm 1.

V. SIMULATION SETTINGS AND RESULTS

A. Simulation Settings

We evaluate the proposed receiver-side decoding framework ICD against conventional SSCC pipelines [13] and representative JSSCC-based semantic communication schemes [56]–[58] over both AWGN and Rayleigh fading channels. To ensure a fair and reproducible comparison, all methods are tested on the same text source and are assessed using widely adopted Natural Language Processing (NLP)-oriented quality metrics [68], [69].

Dataset and source coding. The adopted dataset is the proceedings of the European Parliament [70], which consists of around 2.0 million sentences. The dataset is pre-processed to have sentence lengths ranging from 4 to 30 words for

³FFN denotes the Feed-Forward Network.

Algorithm 1 The Procedure of ICD.

Input: Channel-decoded bitstream $\tilde{\mathbf{m}}$, ECCT-derived reliability $\rho_{\mathbf{m}}$, contextual information \mathbf{m}_{pre} , candidate pool size L_c , sampled subset size L_s , MH steps N_{step} , temperature β , diversity weight λ , fusion weight α ;

Output: Final reconstruction $\tilde{\mathbf{s}}^*$;

- 1: **Stage I: CCG — In-Context Candidate Generator**
- 2: $\mathcal{M} \leftarrow$ constructs candidates $\tilde{\mathbf{m}}$ by Eq. (20).
- 3: $\mathcal{F}_{\text{Conf}}(\tilde{\mathbf{m}}) \leftarrow$ computes confidence scores by Eq. (21)–Eq. (22);
- 4: $\mathcal{M}_{L_c} \leftarrow$ retains top- L_c candidates by Eq. (23);
- 5: **Stage II: CCS — In-Context Candidate Sampler**
- 6: $\mathcal{S}^{(0)} \leftarrow$ initializes a subset in $\Omega = \{\mathcal{S}^{(0)} \subseteq \mathcal{M}_{L_c} \mid |\mathcal{S}^{(0)}| = L_s\}$;
- 7: **for** $t = 0$ to $N_{\text{step}} - 1$ **do**
- 8: $\mathcal{S}^{(t)'} \leftarrow$ generates a proposal state by a single-element replacement in $\mathcal{S}^{(t)}$;
- 9: $\alpha(\mathcal{S}^{(t)} \rightarrow \mathcal{S}^{(t)'}) \leftarrow$ computes the MH acceptance probability by Eq. (28);
- 10: $\mathcal{S}^{(t+1)} \leftarrow$ accepts/rejects $\mathcal{S}^{(t)'}$ according to $u \sim \mathcal{U}(0, 1)$ and $\alpha(\mathcal{S}^{(t)} \rightarrow \mathcal{S}^{(t)'})$;
- 11: **end for**
- 12: $\mathcal{M}_{L_s} \leftarrow$ outputs the selected subset;
- 13: **Stage III: CLR — In-Context Likelihood Ranking**
- 14: $(\tilde{\mathbf{s}}^{(j)}, \ell^{(j)}) \leftarrow$ decodes and computes likelihood with contextual information by Eq. (17);
- 15: $\tilde{\mathbf{s}}^* \leftarrow$ selects the final reconstruction by Eq. (39).

TABLE III
MAIN HYPERPARAMETER SETTINGS USED IN THE EXPERIMENTS.

Model	Hyperparameter	Value
ECCT	Learning rate	10^{-4}
	Batch size	128
	Number of decoder layers	6
	Embedding dimension	32
	Number of attention heads	8
DeepSC	Learning rate	10^{-4}
	Batch size	64
	Number of encoder/decoder layers	4
	Embedding dimension	128
	FFN hidden dimension ³	512
	Number of attention heads	8
UT	Learning rate	10^{-4}
	Batch size	64
	Number of encoder/decoder layers	3
	Embedding dimension	128
	FFN hidden dimension ³	1024
	Number of attention heads	8

training and testing. Unless otherwise stated, we adopt GPT-2 [71] base (124.44M parameters) as the default source model. The arithmetic coder is configured with a precision of 31 bits, which provides a practical trade-off between numerical stability and coding accuracy. For each corpus, some leading words, regarded as the contextual information \mathbf{m}_{pre} , have been correctly decoded.

Channel coding and ECCT configuration. For the SSCC baselines, we employ an LDPC(49, 24) code, corresponding to a code rate of approximately 0.5. The ECCT architecture and training hyperparameters, as well as those of the JSCC baselines, are summarized in Table III.

Baselines. We include the following representative baselines

- Huffman with ECCT, where the LLM-driven arithmetic source coding/decoding is replaced by Huffman coding, while keeping the rest of the SSCC pipeline unchanged.
- LLM-AC with ECCT, which combines ECCT-assisted channel decoding with LLM-based lossless source decoding under the SSCC pipeline.
- DeepSC [56] and UT [57], which serve as representative JSCC baselines for comparison.
- UT with quantization [58], where the continuous latent representation is mapped to a fixed-length bitstream (30 bits) for transmission.

Evaluation metrics. Reconstruction quality is quantified by Bilingual Evaluation Understudy (BLEU) [68] and a Bidirectional Encoder Representations from Transformers (BERT)-based semantic similarity metric [69], which are widely used in text reconstruction tasks to assess lexical fidelity and semantic preservation, respectively.

On the other hand, when comparing heterogeneous pipelines (e.g., SSCC vs. JSCC), different schemes generally transmit different amounts of physical-layer payload N for the same source content. Therefore, to maintain consistent energy accounting, consistent with [13], we normalize SNR using a fixed total transmission energy budget. Let E_{total} denote the total energy consumed by sending N_{um} payload units through the channel in an LLM-based SSCC reference system [13], and define the unified SNR according to

$$\begin{aligned} \text{SNR} &= 10 \log \left(\frac{E_{\text{total}}}{N_0 N} \right) \\ &= 10 \log \left(\frac{E_{\text{total}}}{N_0 N_{\text{um}}} \right) + 10 \log \left(\frac{N_{\text{um}}}{N} \right) \\ &= \text{SNR}_{\text{unified}} + 10 \log \left(\frac{N_{\text{um}}}{N} \right). \end{aligned} \quad (40)$$

Here, $\text{SNR}_{\text{unified}}$ serves as the independent variable that aligns E_{total} across different methodologies, while the ratio N_{um}/N compensates for the differing physical-layer payload lengths. Meanwhile, for JSCC methods such as DeepSC [56] and UT [57], the transmitter commonly outputs continuous latent vectors, and the channel input is represented by floating-point values rather than binary bits. To maintain consistent energy accounting, we treat one transmitted float as consuming the energy of multiple bits. With float16, one float corresponds to 16 bits, resulting in an additional offset $10 \log(16) \approx 12.041$ dB. Accordingly, the unified evaluation metric is given by Eq. (41)

B. Overall System-Level Performance Comparison

Fig. 4 and Fig. 5 present the system-level overall performance comparison between the proposed method and multiple

TABLE IV
MODEL SIZES OF THE LLM BACKBONES.

Model	Parameters (M)
Base model	124.44
Medium model	379.99
Large model	811.78
XL model	1607.94

baselines over AWGN and Rayleigh channels, respectively, evaluated by BLEU-1, BLEU-4, and semantic similarity. The results demonstrate that the proposed receiver-side ICD consistently achieves the best performance in both channel environments, outperforming all baselines. The performance improvement is most evident in the low-SNR regime, where residual bit errors after channel decoding can trigger interval misselection in LLM-driven arithmetic decoding, resulting in a pronounced performance cliff. In this regard, ICD leverages the contextual information to stabilize the initial interval localization and prevent catastrophic early deviation, then constructs multiple bitstream candidates via reliability-guided bit flipping, while a sampling step further enhances candidate diversity and controls decoding overhead.

C. Impact of Confidence-Ranked and Sampled Candidates Hyperparameters

Fig. 6 and Fig. 7 show the BLEU-4 performance of ICD under two coupled hyperparameters, namely the size of the confidence-ranked candidate pool and the number of sampled candidates, which determines how many candidate bitstreams are ultimately decoded. A consistent trend is that using a moderate confidence-ranked pool together with a moderate number of sampled candidates yields the most reliable gains across SNR points. Further increasing the number of sampled candidates does not reliably yield better performance, suggesting that ICD is driven primarily by forming high-quality, reliability-consistent candidates, rather than simply decoding as many candidates as possible. Conversely, using too few sampled candidates under-explores the candidate space and makes ICD more prone to missing the correct interval updating path at low SNR. A similar non-monotonic effect is observed for the confidence-ranked pool size. When the ranked pool is reduced, ICD may discard the true bitstream prematurely, biasing the sampled set toward a narrow subset. By contrast, a larger ranked pool may include additional low-confidence candidates, potentially reducing sampling focus and weakening the reliability-likelihood fusion through less effective exploration.

D. Scalability of the LLM Backbone

We examine how the LLM backbone affects the performance of the proposed ICD framework. Specifically, we evaluate ICD with progressively larger size of LLMs while keeping all other system components unchanged, and the parameter counts of the evaluated backbones are summarized in Table IV. As shown in Fig. 8, consistent but moderate gains are observed

$$\text{SNR} = \begin{cases} \text{SNR}_{\text{unified}} + 10 \log\left(\frac{N_{\text{um}}}{N}\right) + 12.041, & \text{float-based JSCC (float16),} \\ \text{SNR}_{\text{unified}} + 10 \log\left(\frac{N_{\text{um}}}{N}\right), & \text{bit-oriented transmission.} \end{cases} \quad (41)$$

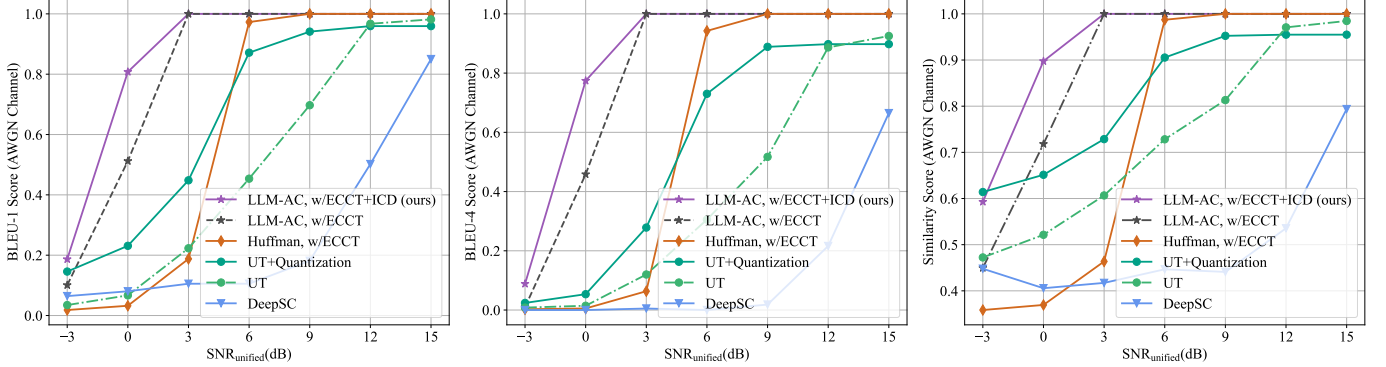


Fig. 4. Overall system-level performance under AWGN channels.

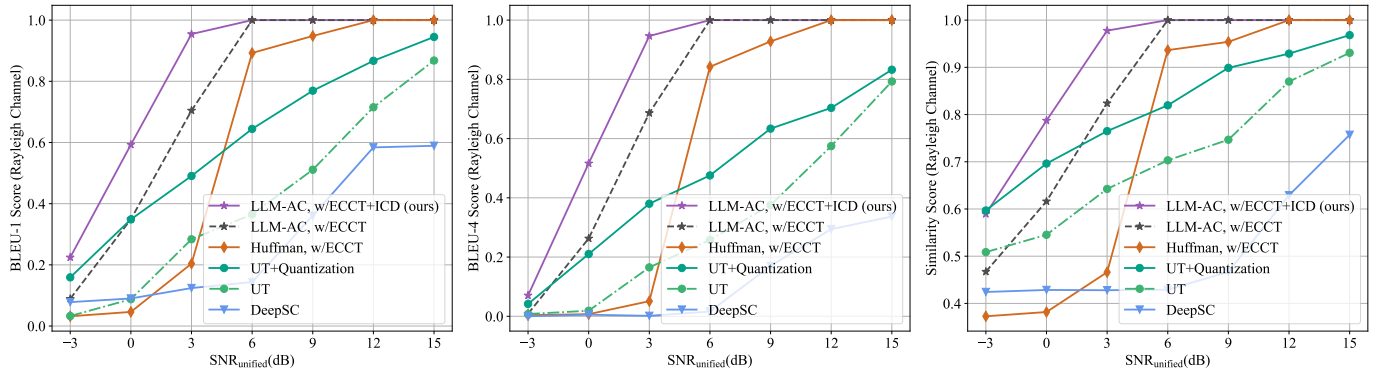


Fig. 5. Overall system-level performance under Rayleigh channels.

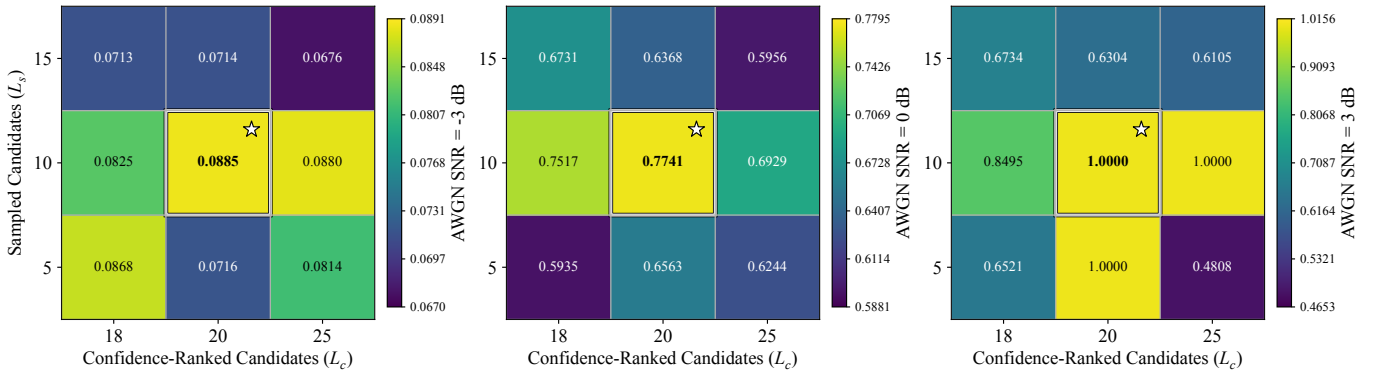


Fig. 6. BLEU-4 heatmaps of ICD performance under AWGN channels.

as the backbone size increases. This trend indicates that ICD can directly benefit from improved language modeling quality, as larger models provide more accurate conditional probability estimates for candidate generation and refinement. At the same time, the performance gap between different model scales remains bounded, suggesting that ICD is largely model-agnostic

and already achieves strong performance with the base model. These results confirm that the proposed framework scales favorably with model capacity while maintaining robustness across different backbone choices.

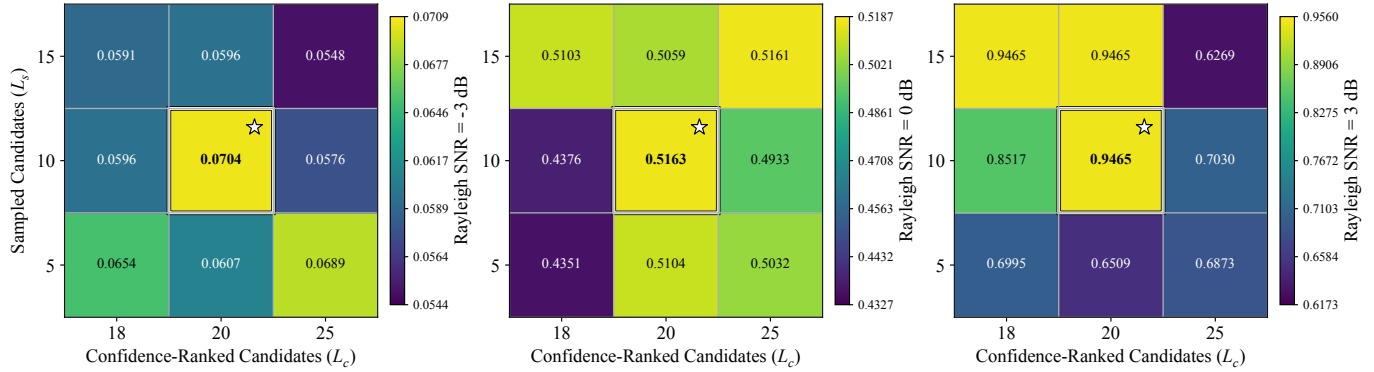


Fig. 7. BLEU-4 heatmaps of ICD performance under Rayleigh channels.

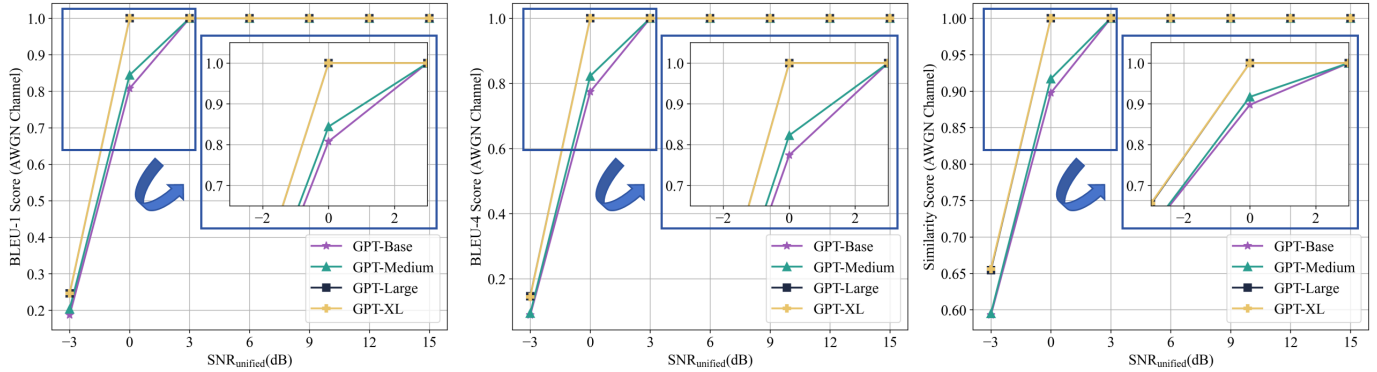


Fig. 8. Scalability evaluation with varying LLM backbone sizes under AWGN channels.

E. Ablation Experiments

Table V presents a comprehensive ablation study under AWGN channels across different code rates and SNRs. Overall, LLM-AC with ECCT+ICD consistently delivers the strongest performance, especially in the low-SNR regimes, where reliable recovery is most challenging. Compared with the ECCT-only baseline, incorporating ICD yields substantial gains across all three metrics, confirming the necessity of structured enhancement beyond ECCT-based decoding. As the code rate increases, performance tends to decline at the same SNR, since higher-rate coding provides less redundancy for error correction and thus leaves more residual errors after decoding, under which the baselines degrade more noticeably while ICD more consistently preserves its advantage.

When the CCS module is removed and only context-assisted decoding is retained (denoted as w/ECCT+Context), performance degrades but remains clearly superior to the ECCT-only baseline. This indicates that context modeling alone provides meaningful improvements, yet is insufficient to fully exploit the candidate space without sampling. The full ICD configuration consistently achieves the best or near-best results, highlighting the complementary roles of context modeling and candidate sampling. We also present a comparison of the runtime test on NVIDIA GeForce RTX 4090 and find that the CCS module yields a $1.6457 \times$ speedup. Overall, it

validates the effectiveness of the CCS module for a more computationally efficient solution.

VI. CONCLUSIONS

In this work, we have presented ICD, a receiver-side in-context decoding framework for improving the robustness of SSCC-based transmission in low-SNR regimes. By leveraging ECCT-derived bit-wise reliability and contextual information, ICD has leveraged a three-stage processing chain composed of CCG, CCS, and CLR. Specifically, CCG has produced a confidence-ranked candidate pool via reliability-guided bit flipping, while CCS has performed diversity-preserving sampling to achieve a favorable accuracy-complexity trade-off, and CLR has fused ECCT-derived reliability with source-level log-likelihood to determine the final reconstruction. We have further provided theoretical guarantees on the stability and convergence of this CCS module. Extensive evaluations over AWGN and Rayleigh fading channels have demonstrated consistent improvements compared with conventional SSCC pipelines and representative JSCC schemes, and achieved a favorable balance between decoding reliability and computational efficiency. In future work, we will extend ICD by incorporating stronger model-free decoding beyond ECCT and develop SSCC designs that better match image modalities for more reliable visual content transmission.

TABLE V
RESULTS UNDER AWGN CHANNELS WITH DIFFERENT CODE RATES.

Code rate (N, K)	SNR (dB)	Method	Metrics		
			BLEU1	BLEU4	Similarity Score
(49,24)	-3	LLM-AC, w/ECCT+ICD	0.1867	0.0885	0.5928
		LLM-AC, w/ECCT+Context	0.1832	0.0714	0.5921
		LLM-AC, w/ECCT	0.1007	0.0097	0.4496
	0	LLM-AC, w/ECCT+ICD	0.8076	0.7741	0.8976
		LLM-AC, w/ECCT+Context	0.6647	0.6135	0.8398
		LLM-AC, w/ECCT	0.5120	0.4584	0.7181
	3	LLM-AC, w/ECCT+ICD	1.0000	1.0000	1.0000
		LLM-AC, w/ECCT+Context	1.0000	1.0000	1.0000
		LLM-AC, w/ECCT	1.0000	1.0000	1.0000
(49,30)	-3	LLM-AC, w/ECCT+ICD	0.1778	0.0708	0.5462
		LLM-AC, w/ECCT+Context	0.1398	0.0530	0.5275
		LLM-AC, w/ECCT	0.0937	0.0093	0.4623
	0	LLM-AC, w/ECCT+ICD	0.5457	0.4833	0.7532
		LLM-AC, w/ECCT+Context	0.5125	0.4429	0.7376
		LLM-AC, w/ECCT	0.3152	0.2322	0.6313
	3	LLM-AC, w/ECCT+ICD	0.9697	0.9602	0.9852
		LLM-AC, w/ECCT+Context	0.9697	0.9602	0.9852
		LLM-AC, w/ECCT	0.9444	0.9266	0.9734
(49,36)	-3	LLM-AC, w/ECCT+ICD	0.1761	0.0480	0.5746
		LLM-AC, w/ECCT+Context	0.1828	0.0485	0.5738
		LLM-AC, w/ECCT	0.0970	0.0090	0.4668
	0	LLM-AC, w/ECCT+ICD	0.4433	0.3602	0.6973
		LLM-AC, w/ECCT+Context	0.2922	0.1719	0.5936
		LLM-AC, w/ECCT	0.1416	0.0478	0.5133
	3	LLM-AC, w/ECCT+ICD	0.9762	0.9674	0.9901
		LLM-AC, w/ECCT+Context	0.8779	0.8455	0.9402
		LLM-AC, w/ECCT	0.6786	0.6093	0.8073

REFERENCES

- [1] K. Lu, *et al.*, “Rethinking modern communication from semantic coding to semantic communication,” *IEEE Wireless Commun.*, vol. 30, no. 1, pp. 158–164, 2023.
- [2] Y. Shao, *et al.*, “A theory of semantic communication,” *IEEE Trans. Mob. Comput.*, vol. 23, no. 12, pp. 12211–12228, Dec. 2024.
- [3] Z. Lu, *et al.*, “Semantics-empowered communications: A tutorial-cum-survey,” *IEEE Commun. Surv. Tutorials*, vol. 26, no. 1, pp. 41–79, Mar. 2024.
- [4] S. Guo, *et al.*, “A survey on semantic communication networks: Architecture, security, and privacy,” *IEEE Commun. Surv. Tutorials*, vol. 27, no. 5, pp. 2860–2894, Oct. 2025.
- [5] A. Vaswani, “Attention is all you need,” in *Proc. Adv. Neural Inf. Proces. Syst., NIPS*, Long Beach, CA, USA, Dec. 2017, p. 6000–6010.
- [6] W. Zhang, *et al.*, “DeepMA: End-to-end deep multiple access for wireless image transmission in semantic communication,” *IEEE Trans. Cognit. Commun. Networking*, vol. 10, no. 2, pp. 387–402, Apr. 2024.
- [7] J. Huang, *et al.*, “D²-JSCC: Digital deep joint source-channel coding for semantic communications,” *IEEE J. Sel. Areas Commun.*, vol. 43, no. 4, pp. 1246–1261, Apr. 2025.
- [8] S. Tong, *et al.*, “Alternate learning-based snr-adaptive sparse semantic visual transmission,” *IEEE Trans. Wireless Commun.*, vol. 24, no. 2, pp. 1737–1752, Feb. 2025.
- [9] J. Wang, *et al.*, “Perceptual learned source-channel coding for high-fidelity image semantic transmission,” in *Proc. IEEE Glob. Commun. Conf., GLOBECOM*, Rio de Janeiro, Brazil, Dec. 2022, pp. 3959–3964.
- [10] C. Bian, *et al.*, “Process-and-forward: Deep joint source-channel coding over cooperative relay networks,” *IEEE J. Sel. Areas Commun.*, vol. 43, no. 4, pp. 1118–1134, Apr. 2025.
- [11] Z. Lyu, *et al.*, “Semantic communications for image recovery and classification via deep joint source and channel coding,” *IEEE Trans. Wireless Commun.*, vol. 23, no. 8, pp. 8388–8404, Aug. 2024.
- [12] Z. Lu, *et al.*, “Self-critical alternate learning-based semantic broadcast communication,” *IEEE Trans. Commun.*, vol. 73, no. 5, pp. 3347–3363, May 2025.
- [13] T. Ren, *et al.*, “Separate source channel coding is still what you need: An llm-based rethinking,” *arXiv preprint arXiv:2501.04285*, 2025.
- [14] J. Huang, *et al.*, “Deep separate source-channel coding for semantic-aware image transmission,” in *Proc. IEEE Int. Conf. Commun., ICC*, Rome, Italy, May 2023, pp. 5626–5631.
- [15] J. Huang, *et al.*, “Joint task and data-oriented semantic communications: A deep separate source-channel coding scheme,” *IEEE Internet Things J.*, vol. 11, no. 2, pp. 2255–2272, Jan. 2024.
- [16] G. Chiarot, *et al.*, “Time series compression survey,” *ACM Comput. Surv.*, vol. 55, no. 10, pp. 1–32, Feb. 2023.
- [17] S. Miao, *et al.*, “Trends in channel coding for 6g,” *Proc. IEEE*, vol. 112, no. 7, pp. 653–675, Jul. 2024.
- [18] G. Delétang, *et al.*, “Language modeling is compression,” *arXiv preprint arXiv:2309.10668*, 2023.
- [19] M. Goyal, *et al.*, “DeepZip: Lossless data compression using recurrent neural networks,” in *Proc. Data Compression Conf., DCC*, Snowbird, UT, USA, Mar. 2019, pp. 575–575.
- [20] Q. Liu, *et al.*, “DecMac: A deep context model for high efficiency arithmetic coding,” in *Proc. Int. Conf. Artif. Intell. Inf. Commun., ICAIIC*, Okinawa, Japan, Feb. 2019, pp. 438–443.
- [21] M. Goyal, *et al.*, “DZip: improved general-purpose loss less compression based on novel neural network modeling,” in *Proc. Data Compression Conf., DCC*, Snowbird, UT, USA, Mar. 2021, pp. 153–162.
- [22] Y. Mao, *et al.*, “TRACE: A fast transformer-based general-purpose lossless compressor,” in *Proc. ACM Web Conf.*, Virtual Edition, Apr. 2022, p. 1829–1838.
- [23] C. S. K. Valmeekam, *et al.*, “Llmzip: Lossless text compression using large language models,” *arXiv preprint arXiv:2306.04050*, 2023.
- [24] C. Huang, *et al.*, “Approximating human-like few-shot learning with gpt-based compression,” *arXiv preprint arXiv:2308.06942*, 2023.

[25] S. S. Narashiman, *et al.*, “AlphaZip: Neural network-enhanced lossless text compression,” *arXiv preprint arXiv:2409.15046*, 2024.

[26] F. Mittu, *et al.*, “Finezip: Pushing the limits of large language models for practical lossless text compression,” *arXiv preprint arXiv:2409.17141*, 2024.

[27] D. A. Huffman, “A method for the construction of minimum-redundancy codes,” *Proc. IRE*, vol. 40, no. 9, pp. 1098–1101, Sep. 1952.

[28] I. H. Witten, *et al.*, “Arithmetic coding for data compression,” *Commun. ACM*, vol. 30, no. 6, p. 520–540, Jun. 1987.

[29] G. Forney, “Convolutional codes i: Algebraic structure,” *IEEE Trans. Inf. Theory*, vol. 16, no. 6, pp. 720–738, Nov. 1970.

[30] R. Bose, *et al.*, “On a class of error correcting binary group codes,” *Inf. Control*, vol. 3, no. 1, pp. 68–79, Mar. 1960.

[31] R. Gallager, “Low-density parity-check codes,” *IRE Trans. Inf. Theory*, vol. 8, no. 1, pp. 21–28, Jan. 1962.

[32] E. Arikan, “Channel polarization: A method for constructing capacity-achieving codes for symmetric binary-input memoryless channels,” *IEEE Trans. Inf. Theory*, vol. 55, no. 7, pp. 3051–3073, Jul. 2009.

[33] J. Guo, *et al.*, “Hard-decision decoding algorithms for ldpc codes based on matching pursuit,” *IEEE Commun. Lett.*, vol. 28, no. 3, pp. 454–457, Mar. 2024.

[34] B. J. Frey, *et al.*, “A revolution: Belief propagation in graphs with cycles,” in *Proc. Adv. Neural Inf. Proces. Syst., NIPS*, Denver, Colorado, USA, Dec. 1997, p. 479–485.

[35] J. Zhao, *et al.*, “On implementation of min-sum algorithm and its modifications for decoding low-density parity-check (LDPC) codes,” *IEEE Trans. Commun.*, vol. 53, no. 4, pp. 549–554, Apr. 2005.

[36] A. Buchberger, *et al.*, “Pruning and quantizing neural belief propagation decoders,” *IEEE J. Sel. Areas Commun.*, vol. 39, no. 7, pp. 1957–1966, Jul. 2021.

[37] G. Larue, *et al.*, “Neural belief propagation auto-encoder for linear block code design,” *IEEE Trans. Commun.*, vol. 70, no. 11, pp. 7250–7264, Nov. 2022.

[38] E. Nachmani, *et al.*, “Autoregressive belief propagation for decoding block codes,” *arXiv preprint arXiv:2103.11780*, 2021.

[39] D. Liu, *et al.*, “Neural belief propagation for scene graph generation,” *IEEE Trans. Pattern Anal. Mach. Intell.*, vol. 45, no. 8, pp. 10161–10172, Aug. 2023.

[40] I. Be’Ery, *et al.*, “Active deep decoding of linear codes,” *IEEE Trans. Commun.*, vol. 68, no. 2, pp. 728–736, Feb. 2020.

[41] F. Liang, *et al.*, “An iterative BP-CNN architecture for channel decoding,” *IEEE J. Sel. Top. Signal Process.*, vol. 12, no. 1, pp. 144–159, Feb. 2018.

[42] Q. Wang, *et al.*, “Normalized min-sum neural network for LDPC decoding,” *IEEE Trans. Cognit. Commun. Networking*, vol. 9, no. 1, pp. 70–81, Feb. 2023.

[43] H.-Y. Kwak, *et al.*, “Boosting learning for LDPC codes to improve the error-floor performance,” in *Proc. Adv. Neural Inf. Proces. Syst., NIPS*, New Orleans, LA, USA, Dec. 2023, pp. 22 115–22 131.

[44] T. Gruber, *et al.*, “On deep learning-based channel decoding,” in *Proc. Annu. Conf. Inf. Sci. Syst., CISS*, Baltimore, MD, USA, Mar. 2017, pp. 1–6.

[45] E. U. Kargi, *et al.*, “A deep learning based decoder for concatenated coding over deletion channels,” in *Proc. IEEE Int. Conf. Commun., ICC*, Denver, CO, USA, Jun. 2024, pp. 2797–2802.

[46] S. A. Hebbar, *et al.*, “CRISP: Curriculum based sequential neural decoders for polar code family,” in *Proc. Int. Conf. Machin. Learn., ICML*, Honolulu, Hawaii, USA, Jul. 2023, pp. 12 823–12 845.

[47] G. De Boni Rovella, *et al.*, “Improved syndrome-based neural decoder for linear block codes,” in *Proc. IEEE Glob. Commun. Conf., GLOBECOM*, Kuala Lumpur, Malaysia, Dec. 2023, pp. 5689–5694.

[48] Y. Choukroun, *et al.*, “Error correction code transformer,” in *Proc. Adv. Neural Inf. Proces. Syst., NIPS*, New Orleans, LA, USA, Nov. 2022, pp. 38 695–38 705.

[49] S.-J. Park, *et al.*, “Multiple-masks error correction code transformer for short block codes,” *IEEE J. Sel. Areas Commun.*, vol. 43, no. 7, pp. 2518–2529, Jul. 2025.

[50] H. Xie, *et al.*, “Semantic communication with memory,” *IEEE J. Sel. Areas Commun.*, vol. 41, no. 8, pp. 2658–2669, 2023.

[51] D. Gündüz, *et al.*, “Beyond transmitting bits: Context, semantics, and task-oriented communications,” *IEEE J. Sel. Areas Commun.*, vol. 41, no. 1, pp. 5–41, 2023.

[52] Y. Liu, *et al.*, “Extended context-based semantic communication system for text transmission,” *Digital Commun. Networks*, vol. 10, no. 3, pp. 568–576, 2024.

[53] Y. Ren, *et al.*, “A sequence repetition node-based successive cancellation list decoder for 5g polar codes: Algorithm and implementation,” *IEEE Trans. Signal Process.*, vol. 70, pp. 5592–5607, 2022.

[54] I. Sagitov, *et al.*, “Generalized restart mechanism for successive-cancellation flip decoding of polar codes,” *J. Signal Process. Syst.*, vol. 97, pp. 11–29, 2025.

[55] C. Meister, *et al.*, “Locally typical sampling,” *Trans. Assoc. Comput. Linguist.*, vol. 11, pp. 102–121, 2023.

[56] H. Xie, *et al.*, “Deep learning enabled semantic communication systems,” *IEEE Trans. Signal Process.*, vol. 69, pp. 2663–2675, Apr. 2021.

[57] Q. Zhou, *et al.*, “Semantic communication with adaptive universal transformer,” *IEEE Wireless Commun. Lett.*, vol. 11, no. 3, pp. 453–457, Mar. 2022.

[58] Q. Zhou, *et al.*, “Adaptive bit rate control in semantic communication with incremental knowledge-based HARQ,” *IEEE Open J. Commun. Soc.*, vol. 3, pp. 1076–1089, Jul. 2022.

[59] F. Zhou, *et al.*, “Cognitive semantic communication systems driven by knowledge graph: Principle, implementation, and performance evaluation,” *IEEE Trans. Wireless Commun.*, vol. 72, no. 1, pp. 193–208, 2024.

[60] A. Kurmukova, *et al.*, “Friendly attacks to improve channel coding reliability,” in *Proc. AAAI Conf. Artif. Intell., AAAI*, Vancouver, Canada, Feb. 2024, pp. 13 292–13 300.

[61] L. Zhang, *et al.*, “Unsupervised learning for ultra-reliable and low-latency communications with practical channel estimation,” *IEEE Trans. Wireless Commun.*, vol. 23, no. 4, pp. 3633–3647, Apr. 2024.

[62] M. E. Haque, *et al.*, “A comprehensive survey of 5G URLLC and challenges in the 6G era,” *arXiv preprint arXiv:2508.20205*, 2025.

[63] J. Xue, *et al.*, “Cooperative deep reinforcement learning enabled power allocation for packet duplication URLLC in multi-connectivity vehicular networks,” *IEEE Trans. Mob. Comput.*, vol. 23, no. 8, pp. 8143–8157, Aug. 2024.

[64] G. R. A. Faria, *et al.*, “QUEST: Quality-aware metropolis-hastings sampling for machine translation,” in *Proc. Adv. Neural Inf. Proces. Syst., NIPS*, Vancouver, Canada, Dec. 2024, pp. 89 042–89 068.

[65] A. Karan, *et al.*, “Reasoning with sampling: Your base model is smarter than you think,” *arXiv preprint arXiv:2510.14901*, 2025.

[66] D. A. Levin, *et al.*, *Markov chains and mixing times*. American Mathematical Soc., 2017.

[67] J. R. Norris, *Markov Chains*. Cambridge University Press, 1998.

[68] K. Papineni, *et al.*, “BLEU: a method for automatic evaluation of machine translation,” in *Proc. ACL*, Philadelphia, Pennsylvania, USA, Jul. 2002, pp. 311–318.

[69] J. Devlin, *et al.*, “BERT: Pre-training of deep bidirectional transformers for language understanding,” in *Proc. Conf. N. Am. Chapter Assoc. Comput. Linguistics: Hum. Lang. Technol.*, Minneapolis, Minnesota, Jun. 2019, pp. 4171–4186.

[70] P. Koehn, “Europarl: A parallel corpus for statistical machine translation,” in *Proc. MTSummit*, Phuket, Thailand, Sep. 2005, pp. 79–86.

[71] A. Radford, *et al.*, “Language models are unsupervised multitask learners,” OpenAI Technical Report, 2019, [Online]. Available: https://cdn.openai.com/better-language-models/language_models_are_unsupervised_multitask_learners.pdf. [Online]. Available: https://cdn.openai.com/better-language-models/language_models_are_unsupervised_multitask_learners.pdf